Depletion of Adipocyte *Becn1* Leads to Lipodystrophy and Metabolic Dysregulation

Young Jin,[1] Yul Ji,[2] Yaechan Song,[1] Sung Sik Choe,[2] Yong Geun Jeon,[2] Heeju Na,[1] Tae Wook Nam,[1] Hye Jeong Kim,[1] Hahn Nahmgoong,[2] Sung Min Kim,[2] Jae-woo Kim,[3] Ki Taek Nam,[4] Je Kyung Seong,[5] Daehee Hwang,[6] Chan Bae Park,[7] In Hye Lee,[8] Jae Bum Kim,[2] and Han-Woong Lee[1]

Diabetes 2021;70:182–195 | https://doi.org/10.2337/db19-1239

***Becn1/Beclin-1* is a core component of the class III phosphatidylinositol 3-kinase required for autophagosome formation and vesicular trafficking. Although *Becn1* has been implicated in numerous diseases such as cancer, aging, and neurodegenerative disease, the role of *Becn1* in white adipose tissue and related metabolic diseases remains elusive. In this study, we show that adipocyte-specific *Becn1* knockout mice develop severe lipodystrophy, leading to adipose tissue inflammation, hepatic steatosis, and insulin resistance. Ablation of *Becn1* in adipocytes stimulates programmed cell death in a cell-autonomous manner, accompanied by elevated endoplasmic reticulum (ER) stress gene expression. Furthermore, we observed that *Becn1* depletion sensitized mature adipocytes to ER stress, leading to accelerated cell death. Taken together, these data suggest that adipocyte *Becn1* would serve as a crucial player for adipocyte survival and adipose tissue homeostasis.**

Adipose tissue plays a crucial role in the regulation of metabolic homeostasis through cross talk with other metabolic tissues. Adipose tissue is expanded by two processes, formation of new adipocytes (hyperplasia) and enlargement of existing adipocytes (hypertrophy) (1). In response to nutritional states, adipose tissue can dynamically increase its lipid storage capacity through hypertrophic expansion to accommodate excess nutrients. Besides, adipocyte hyperplasia is known to contribute to the healthy expansion of adipose tissue. In obesity, however, adipocyte hypertrophy often promotes adipocyte cell death, thereby leading to adipose tissue inflammation and systemic insulin resistance (2).

Adipose tissue dysregulation, as observed in obesity, is closely associated with metabolic complications, including insulin resistance, hepatic steatosis, and diabetes (3). In contrast, lipodystrophies, caused by genetic and environmental factors, are characterized by complete or partial loss of adipose tissue and can also lead to metabolic diseases. For example, congenital generalized lipodystrophy, which is caused by inherited *AGPAT2*, *BSCL2*, *CAV1*, or *PTRF* mutations, promotes metabolic alterations, such as insulin resistance, dyslipidemia, and hepatic steatosis (4). In addition, multiple nongenetic factors are often involved in acquired lipodystrophies caused by antiretroviral treatment of HIV, autoimmunity, or unknown reasons (5,6). Notably, the severity of lipodystrophy is often correlated with a loss of adipose mass caused by adipocyte death (1,7). Thus, it is imperative to understand the underlying mechanisms responsible for

[1]Department of Biochemistry, College of Life Science and Biotechnology, Yonsei University, Seoul, Republic of Korea
[2]Department of Biological Sciences, Center for Adipocyte Structure-Function, Institute of Molecular Biology and Genetics, Seoul National University, Seoul, Republic of Korea
[3]Department of Biochemistry and Molecular Biology, Brain Korea 21 PLUS Project for Medical Science, Yonsei University College of Medicine, Seoul, Republic of Korea
[4]Severance Biomedical Science Institute, Brain Korea 21 PLUS Project for Medical Science, Yonsei University College of Medicine, Seoul, Republic of Korea
[5]Korea Mouse Phenotyping Center, Seoul National University, Seoul, Republic of Korea
[6]Department of Biological Sciences, Seoul National University, Seoul, Republic of Korea
[7]Department of Physiology, Ajou University School of Medicine, Suwon, Republic of Korea
[8]Department of Life Sciences, Ewha Womans University, Seoul, Republic of Korea

Corresponding author: Jae Bum Kim, jaebkim@snu.ac.kr, or Han-Woong Lee, hwl@yonsei.ac.kr

Received 22 December 2019 and accepted 2 October 2020

This article contains supplementary material online at https://doi.org/10.2337/figshare.13043093.

Y. Jin, Y. Ji, and Y.S. contributed equally to this work.

adipocyte survival and maintenance of adipose tissue homeostasis, which are critical for systemic energy metabolism.

Macroautophagy (referred to in this article as autophagy) is the catabolic process that delivers damaged and unnecessary cytosolic contents to lysosomes for degradation. Autophagic removal of defective subcellular organelles and long-lived proteins is of great importance for cell survival. Although appropriate autophagic machinery is required for survival, it can also mediate apoptosis in the absence of core apoptotic machinery (8). In mammals, several studies in knockout (KO) mice for autophagy-related (*Atg*) genes revealed that autophagy could regulate adipocyte differentiation and beigeing/browning of adipose tissue (9–11). For example, adipocyte-specific *Atg7* KO mice (aP2-*Cre*-*Atg7*$^{f/f}$) exhibited reduced fat mass with attenuated white fat cell differentiation, but showed an increased number of beige adipocytes (9,10). Selective ablation of *Atg12* or *Atg5* driven by uncoupling protein 1 promoter also revealed that autophagy-mediated mitochondrial clearance is critical for beige adipocyte maintenance by inhibiting the beige-to-white fat transition (11). Consequently, it has been suggested that inhibition of autophagy could be a therapeutic strategy to counteract obesity via promoting beigeing/browning of white adipose tissue (WAT) (11). As autophagy has been implicated in adipogenesis and beige-to-white fat transition, growing interest has emerged to identify its role in mature adipocytes. Moreover, recent studies have revealed that defective autophagy completion could cause failure in maintaining adipose tissue homeostasis and lipid metabolism. For instance, adipocyte-specific *Atg3* and *Atg16L1* deletion induces mitochondrial defects, accompanied by heterogeneous adipocyte size and decreased adipocyte number, resulting in dysregulated lipid metabolism (12). Nevertheless, underlying mechanisms by which autophagy-related genes could affect adipose tissue homeostasis remain elusive.

Becn1/*Beclin-1*, the ortholog of yeast *Atg6*, is a haploinsufficient tumor suppressor gene that acts as a regulator of the class III phosphatidylinositol 3-kinase complex, which is involved in autophagosome formation and membrane trafficking (13). It has been demonstrated that the cross talk between apoptosis and autophagy is regulated by *Becn1*. For instance, as the binding partner of *Bcl-2*, one of the well-known antiapoptotic mediators, *Becn1* is a key determinant as to whether cells are resistant to apoptosis or autophagy under pathophysiological conditions (14). *Becn1* is also involved in metabolic regulation as well as cell survival. Whereas *Becn1*$^{+/-}$ mice did not exhibit obvious metabolic defects compared with wild-type (WT) mice (15), a recent report with *Becn1*^{F121A} knockin mice, in which *Becn1* is hyperactivated, suggests that *Becn1*-mediated autophagy hyperactivation differentially regulates insulin sensitivity in a tissue-dependent manner (16). While dysregulation of *Becn1*-mediated autophagy would be involved in metabolic disorders, underlying physiological roles of *Becn1* in adipocytes are not fully elucidated.

In this study, we generated and characterized adipocyte-specific *Becn1* KO mice using the Adipoq-*Cre* line. Adipocyte-specific *Becn1* KO mice showed severe lipodystrophy associated with adipose tissue inflammation, insulin resistance, hyperglycemia, fatty liver, and a higher risk of death. Further, the ablation of *Becn1* in adipocytes resulted in adipocyte cell death in a cell-autonomous manner, leading to adipose tissue inflammation and insulin resistance. Also, we found that *Becn1* KO adipocytes exhibited elevated endoplasmic reticulum (ER) stress–related gene expression to stimulate apoptotic signals, mediating that *Becn1* would be important for adipocyte survival. These data suggest that *Becn1* plays a key role in maintaining adipose tissue homeostasis and systemic metabolic regulation.

RESEARCH DESIGN AND METHODS

Animals Used in the Study

Adipoq-Cre (JAX stock number 010803) and β-actin–FLPe (JAX stock number 005703) were obtained from The Jackson Laboratory. *Becn1*$^{tm1a(KOMP)Wtsi}$ mice (project identification number CSD 38776) were obtained from the Knockout Mouse Project repository. Mice used in studies were maintained in a C57BL/6JBomTac genetic background and housed in a controlled environment with a 12-h light/dark cycle. Male mice were fed either a normal chow diet (NCD) or high-fat diet (HFD) for indicated times and provided with free access to food and water. Body composition was analyzed by nuclear magnetic resonance using a Bruker Minispec LF50 (Bruker, Hamburg, Germany). Animal care and experiments were performed in accordance with the guidelines of the Korean Food and Drug Administration and were approved by the Institutional Animal Care and Use Committees of the Laboratory Animal Research Center at Yonsei University (permit number 201702-157-02). Mice were maintained in the specific pathogen-free facility of the Yonsei Laboratory Animal Research Center.

Generation of KO Mice

The KO first allele (tm1a) of *Becn1* contains a lacZ-trapping cassette and a neo cassette inserted into the intron 3 of *Becn1* (Supplementary Fig. 1). Mice containing the floxed allele were generated by crossing *Becn1*$^{tm1a(KOMP)Wtsi}$ mice with β-actin–*Flpe*–transgenic mice to remove the gene-trap cassette. The resulting excised alleles were validated by PCR analysis using genomic DNA extracted from mouse tail tips. Homozygous *Becn1*$^{f/f}$ mice were then crossed with Adipoq-*Cre*–transgenic mice to delete exons 4–7 of *Becn1*, triggering nonsense-mediated decay of the transcript by a frame-shift mutation.

Genomic DNA Extraction and Genotyping

Mouse tail biopsies were lysed overnight at 55°C in a buffer (50 mmol/L Tris, pH 8.0, 50 mmol/L EDTA, pH 8.0, 0.5% SDS, and protein kinase K). On the following day, genomic DNA was extracted from the lysates by the phenol-chloroform method. For routine genotyping, the following primers were used for detecting both WT and

floxed alleles: P1-forward (5′-GCTTAGGTCTGA CTGGGTCG-3′) and P2-reverse (5′-ACCCAGGCAAGTGTGTTTTC-3′). For confirming deleted *Becn1* alleles, the following primers were used: P3-forward (5′-TTGTACCGTGATTTAGGGCGTTTGC-3′) and P2-reverse (5′-ACCCAGGCAAGTGTGTTTTC-3′).

Western Blotting and Antibodies

Western blotting was performed as described previously (17) with slight modifications. Mouse tissue was homogenized in radioimmunoprecipitation assay buffer (50 mmol/L Tris pH 7.4, 150 mmol/L NaCl, 1% Nonidet P-40, 0.5% deoxycholate, 0.1% SDS, 1 mmol/L EDTA, pH 8.0, and protease inhibitor cocktail). The samples were incubated with the following primary antibodies: anti-BECN1 (#3738; Cell Signaling Technology), anti-AKT (#9272; Cell Signaling Technology), anti–phospho-AKT (#9271; Cell Signaling Technology), anti-FABP4 (#2120; Cell Signaling Technology), anti-FASN (#3180; Cell Signaling Technology), anti-PPARγ (#2435; Cell Signaling Technology), anti-PLIN1 (#9349; Cell Signaling Technology), anti-CHOP (#2895; Cell Signaling Technology), anti-BIM (#2933; Cell Signaling Technology), anti-BAX (sc-493; Santa Cruz Biotechnology), anti-BCL2 (sc-7382; Santa Cruz Biotechnology), anti-ubiquitin (sc-166553; Santa Cruz Biotechnology), anti-PERK (#3192; Cell Signaling Technology), anti-IRE1α (ab48187; Abcam), anti-eIF2a (sc517214; Santa Cruz Biotechnology), anti–phospho-eIF2a (#9721; Cell Signaling Technology), anti-actin (sc-47778; Santa Cruz Biotechnology), anti-GAPDH (sc-32233; Santa Cruz Biotechnology), anti-LC3 (L8918; Sigma-Aldrich), anti-p62 (H00008878-M01; Abnova), and anti-GRP78 (ab21685; Abcam). After incubation with the primary antibodies, the membranes were incubated with the appropriate peroxidase-conjugated secondary antibodies (GenDEPOT). Protein expression was detected by enhanced chemiluminescence reagents and LAS-3000 image analyzer (Fujifilm, Tokyo, Japan).

Glucose and Insulin Tolerance Tests

For glucose tolerance tests (GTTs) and insulin tolerance tests (ITTs), mice were fasted for 6 h and then received an intraperitoneal injection of 20% glucose (2 g/kg body weight) or human insulin (0.75 units/kg body weight). Blood samples were collected from the tail tips at the indicated time points for glucose measurement. The blood glucose was measured using a glucometer AGM-3000 (GlucoDr Plus; Allmedicus, Gyeonggi-do, Republic of Korea).

Histology

Tissue samples were fixed in 10% formalin (#HT501640; Sigma-Aldrich) and then incubated overnight. Samples were dehydrated and embedded in paraffin using an automated tissue processor (Leica TP1020; Leica Biosystems, Newcastle upon Tyne, U.K.). The sections (4–5-μm thick) were deparaffinized and stained with hematoxylin and eosin (H&E) or taken for immunohistochemistry analysis. For immunohistochemistry analysis, the sections were incubated overnight with the primary antibody PLIN1 (20R-PP004; Fitzgerald Industries), CD11b (14-0112-81; eBioscience), CD11c (14-0114-81; eBioscience), and BAX (sc-23959; Santa Cruz Biotechnology). Secondary antibodies conjugated to horseradish peroxidase or a fluorescent molecule were applied for detection. The TUNEL assay was performed using the ApopTag Fluorescein In Situ Apoptosis Detection Kit (S7110; Millipore). To quantify the adipocyte areas, >800 adipocytes/mouse were counted from images of histological sections and then analyzed using the *Adiposoft* software (18).

Metabolic Parameters

Blood was obtained from the retro-orbital sinus using heparinized capillary tubes. Serum insulin levels were measured by a mouse insulin ELISA kit (AKRIN-011T; Shibayagi Corporation, Gunma, Japan). Serum triglyceride (TG) and total cholesterol were measured by a Dri-Chem 4000i (Fujifilm). Serum free fatty acid (FFA) (K612; BioVision Inc.) and β-hydroxybutyrate (β-HB) (K632; BioVision Inc.) were measured according to the manufacturer's instructions.

RNA Extraction and Quantitative RT-PCR Analysis

Total RNA was extracted from the tissues and cells using TRIzol Reagent (#15596026; Invitrogen) and RNeasy Mini Kit (#74104; Qiagen, Hilden, Germany). First-strand cDNA was prepared from 500 ng of total RNA using RevertAid First Strand cDNA Synthesis (#K1622; Thermo Fisher Scientific) according to the manufacturer's instructions. The quantitative RT-PCR (qRT-PCR) analysis was performed using primers listed in Supplementary Table 1. Samples were analyzed on a CFX Connect Real-Time PCR Detection System (Bio-Rad) and normalized to *Ppia* or *Tbp1* expression.

Adipose Tissue Fractionation

Adipose tissue was fractionated as previously described (19). Briefly, epididymal WAT (eWAT) and inguinal WAT (iWAT) of mice were isolated, dissected out, chopped, and incubated in collagenase buffer (0.1 mol/L HEPES, 0.125 mol/L NaCl, 5 mmol/L KCl, 1.3 mmol/L $CaCl_2$, 5 mmol/L glucose, 1.5% [w/v] glucose, and 0.1% [w/v] collagenase I) for 20 min at 37°C with shaking. Cell suspensions were centrifuged and then washed twice. Supernatants containing adipocytes were used for Western blot analysis. Pelleted stromal vascular cell (SVC) fractions were used for flow cytometry and SVC-derived adipocyte differentiation.

SVC-Derived Adipocyte Differentiation

Preadipocytes were grown to confluence (day 0) in the induction medium consisting of DMEM, 10% FBS, 167 nmol/L insulin, 1 μmol/L 3,3′,5-triiodo-L-thyronine (T3), 2 μmol/L rosiglitazone, 520 μmol/L isobutylmethylxanthine, and 1 μmol/L dexamethasone. After a 2-day incubation in the induction medium, the cells were transferred to a differentiation medium (DMEM, 10% FBS,

167 nmol/L insulin, 1 μmol/L T3, and 2 μmol/L rosiglitazone), which was changed every other day.

SVC Immortalization and *Becn1* Conditional KO

Human embryonic kidney 293 (HEK293) cells were transfected with simian virus 40 large T antigen containing plasmid using Lipofectamine. Media was then harvested 40 h post-transfection. The virus-containing media in the presence of polybrene (5 μg/mL) was treated to SVCs extracted from mice mated with Becn1$^{f/f}$ and ROSA-Cre^{ERT2}. Six to 8 h later, the viral supernatant was removed and reinfected for another day. SVCs immortalized using simian virus 40 T antigen (imSVCs) were selected based on adipocyte differentiation efficiency. Once terminal differentiation occurs (day 8), imSVCs were treated with tamoxifen (500 nmol/L, 72 h) to knock out *Becn1*.

ER Stress Induction and Inhibition

Tunicamycin (SML1287) was purchased from Sigma-Aldrich. Five μmol/L of tunicamycin was treated to mature adipocytes in culture for indicated days. Taurosodeoxycholic acid (TUDCA) (580549) was purchased from Millipore. A total of 400 μmol/L was treated to mature adipocytes in culture for the indicated days.

Flow Cytometry

Flow cytometric analysis was performed as previously described (20). SVC fractions were separated from red blood cells by adding lysis buffer (155 mmol/L NH_4Cl/0.1 mol/L Tris-HCl [pH 7.65] [9:1]). SVCs were stained with monoclonal antibodies against CD11b (27-0112-81; eBioscience), F4/80 (45-4801-80; eBioscience), CD11c (12-0114-82; eBioscience), and CD206 (123009; BioLegend) for macrophage analysis using an FACSCanto II (BD Biosciences).

Luciferase Assay

HEK293 cells were transiently transfected with various DNA plasmids (PPARγ, RXRα, β-galactosidase, and DR-1) by the calcium phosphate method, as previously described (21). Luciferase and β-galactosidase activities were measured according to the manufacturer's instructions (Promega). Relative luciferase activity was normalized to β-galactosidase activity in each sample.

Statistical Analysis

Data are presented as mean ± SEM. Results were analyzed using GraphPad Prism 5 software. Unpaired Student *t* test was used to compare two groups, while two-way ANOVA was used to compare more than two groups. A repeated-measures ANOVA was used for analysis of body weight, GTT, and ITT data. A Bonferroni post hoc test was used to test for significant differences as determined by the ANOVA. A P value <0.05 was considered statistically significant.

Data and Resource Availability

The data sets generated during the current study are available from the corresponding author on reasonable request.

RESULTS

Generation of Adipocyte-Specific *Becn1* KO Mice

To investigate the role of *Becn1* in adipose tissue, we generated adipocyte-specific *Becn1* KO mice by crossing floxed *Becn1* mice with Adipoq-*Cre* mice (Supplementary Fig. 1*A* and *B*) (Adipoq-*Cre*$^{Tg/+}$; *Becn1*$^{f/f}$, hereafter referred to as AKO). Littermates of Adipoq-*Cre*$^{+/+}$; *Becn1*$^{f/f}$ (hereafter referred to as WT) mice were used as controls. Western blot analyses revealed that BECN1 expression was decreased in the adipocytes of AKO mice, with impaired autophagic flux as indicated by autophagy markers such as p62, ubiquitin, and LC3 (Fig. 1*A*). However, there were no significant differences in *Becn1* expression and autophagic flux in nonadipose tissues such as liver and skeletal muscle between WT and AKO mice (Fig. 1*A*), indicating that *Becn1* is specifically depleted in adipose tissue of AKO mice.

Loss of WAT Mass in *Becn1* AKO Mice

Even though there were no significant differences in body weights between WT and AKO mice (Fig. 1*B*), WAT mass of AKO mice was dramatically lower, while lean mass was significantly higher (Fig. 1*C*). As shown in Fig. 1*D*, iWAT and eWAT of AKO mice were reduced by 61.9% and 80.8%, respectively (Fig. 1*D*). The decrease in eWAT mass of AKO mice closely correlated with a high frequency of small adipocytes (Fig. 1*E*). This tendency was enhanced upon aging (Supplementary Fig. 1*C*). Nevertheless, there was no significant difference in food and water intake between the two genotypes (Supplementary Fig. 1*D* and *E*). Accordingly, a significant decrease in mRNA expression of key adipogenic markers including *Pparγ2* (~2.5-fold), *C/ebpα* (~1.8-fold), *Plin1* (~3.1-fold), *Fabp4* (~2.2-fold), and *Adipoq* (~2.6-fold) was observed in AKO mice (Fig. 1*F*). These results were further confirmed by Western blot analyses of the adipogenic markers (Fig. 1*G*). In contrast, the mass and size of the livers in AKO mice were significantly higher (Fig. 1*H*), which could contribute to an increase in the lean mass. As adipose tissues in AKO mice were unable to store lipid, there could be ectopic lipid deposition in the liver. Indeed, the livers of aged AKO mice were grossly enlarged and appeared pale yellow (Fig. 1*I*). Moreover, histological examination confirmed substantial lipid accumulation in the liver of AKO mice (Fig. 1*I*). These data reveal that *Becn1* deficiency in adipose tissue promotes WAT reduction, accompanied by ectopic lipid accumulation in the liver.

Increased Adipose Tissue Inflammation in *Becn1* AKO Mice

Compared with WT littermates, AKO mice exhibited smaller adipocytes in eWAT with a larger eosinophilic cytoplasm

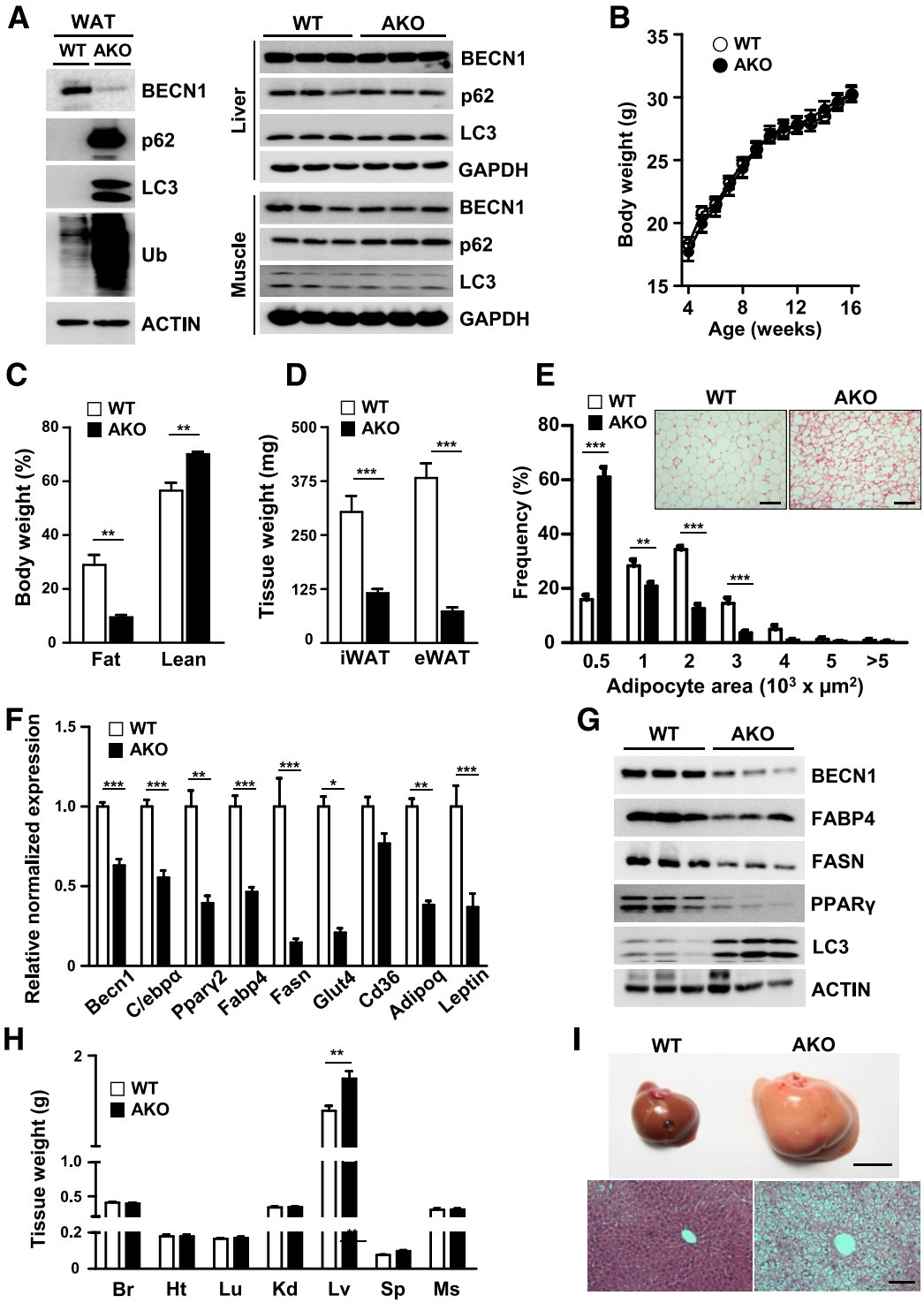

Figure 1—Adipocyte *Becn1* deficiency reduces WAT mass. *A* (left panel): Western blot analysis of protein lysates isolated from adipocytes of eWAT from adipocyte-specific *Becn1* WT and AKO mice. *A* (right panel): Western blot analysis of BECN1, p62, and LC3 expression in protein lysates from the liver and muscle of WT and AKO mice. *B*: Body weight changes in chow-fed WT and AKO mice from 4 to 16 weeks of age (n = 11). *C*: Fat and lean mass from WT and AKO mice (n = 3), measured by nuclear magnetic resonance–based body composition analysis. *D*: Tissue weight of iWAT and eWAT from 10-week-old WT and AKO mice (n = 10). *E*: The cell area distribution of adipocytes from 10-week-old *Becn1* WT and AKO mice (n = 8). The adipocyte area was calculated from eWAT of mice using the *Adiposoft* software. Scale bars, 100 μm. *F*: The mRNA expression levels of fat differentiation markers in eWAT from 10-week-old WT and AKO mice (n = 7). The qRT-PCR results were normalized to *Ppia*. *G*: Western blot analysis of protein lysates from eWAT of 12-week-old WT and AKO mice. Data are presented as mean ± SEM. *H*: Tissue weight of nonadipogenic tissues from 10-week-old WT and AKO mice (n = 10). *I* (top panel): Morphological analysis of the liver from 6-month-old WT and AKO mice. Scale bar, 1 cm. *I* (bottom panel): H&E staining of the liver from 6-month-old WT and AKO mice. Scale bar, 100 μm. Data are presented as mean ± SEM. $^*P < 0.05$; $^{**}P < 0.01$; $^{***}P < 0.001$. Br, brain; Ht, heart; Lu, lung; Kd, kidney; Lv, liver; Ms, muscle; Sp, spleen; Ub, ubiquitin.

(Fig. 2*A*). Moreover, crownlike structures (CLSs) were frequently observed in AKO mice, indicating increased dead or dying adipocytes with macrophage infiltration (Fig. 2*A* and *B*). Consistently, the mRNA levels of macrophage genes such as *F4/80*, *Cd11b*, and *Cd11c* were elevated in eWAT of AKO mice (Fig. 2*C*). Enhanced infiltration of monocytes/macrophages in eWAT of AKO mice was assessed by staining with antibodies for CD11b and CD11c and measuring fluorescence intensity in the histological analysis (Fig. 2*D*). It is well known that HFD-induced obese mice show greatly elevated M1-like proinflammatory macrophage infiltration in eWAT (22). It is of interest to note that NCD-fed AKO mice showed higher mRNA expression of both M1 (*Tnf-α* and *Mcp-1*) and M2 markers (*CD206* and *Il-10*) in eWAT (Fig. 2*E*), implying that eWAT of AKO mice appeared to be vulnerable to macrophage infiltration. Consistently, FACS of SVCs isolated from eWAT of WT and AKO mice showed that the number of F4/80 and CD11b double-positive macrophages was significantly higher in AKO mice (Fig. 2*F*). In eWAT of AKO mice, numbers of both M1-like (F4/80, CD11b, and CD11c triple-positive) and M2-like (F4/80, CD11b, and CD206 triple-positive and CD11c-negative) adipose tissue macrophages (ATMs) were elevated (Fig. 2*G*). These results suggest that the ablation of *Becn1* in adipocytes potently induces adipose tissue inflammation through infiltration of both M1-like and M2-like ATMs.

Effects of HFD on *Becn1* AKO Mice

Obesity is characterized by imbalanced expansion and chronic inflammation in adipose tissue. To determine the effects of adipocyte *Becn1* deficiency on the pathological remodeling of adipose tissue in obesity, an HFD challenge was performed. Compared with HFD-fed WT littermates, HFD-fed AKO mice exhibited much less body weight gain and severely restricted increase of eWAT and iWAT mass (Supplementary Fig. 2*A* and *B*). When HFD-fed WT and AKO mice were subjected to tests with metabolic cages, AKO mice did not show significant difference in respiratory exchange ratio, food intake, or energy expenditure (Supplementary Fig. 2*C*–*E*). In contrast, we observed severe inflammatory response in adipose tissue. As indicated in Supplementary Fig. 2*H* and *I*, eWAT of AKO mice contained more ATMs with either NCD or HFD. Although macrophage infiltration is more frequently observed in eWAT than iWAT upon HFD, significant infiltration of macrophages was also observed in iWAT of HFD-fed AKO mice (Supplementary Fig. 2*J*), accompanied by a higher percentage of M1-like macrophages and M1/M2 ratio in the SVCs (Supplementary Fig. 2*K* and *L*).

Dysfunctional Adipose Tissue in *Becn1* AKO Mice

We next examined the serum profiles of WT and AKO mice under different nutritional states, such as feeding and fasting conditions. While fed WT and AKO mice showed no significant changes in serum levels of TG, FFA, as well as β-HB, fasted AKO mice revealed significantly lower serum levels of TG (~68.3%), FFA (~73.6%), and β-HB (~53.3%) (Fig. 3*A*). As lipodystrophy is often accompanied by insulin resistance and glucose intolerance (23), we could also observe that compared with WT mice, AKO mice showed elevated blood glucose levels during a fasting state (Fig. 3*B*). Also, serum insulin levels of AKO mice were significantly higher than those of WT mice (Fig. 3*C*). Further, high levels of HOMA of insulin resistance indicated that AKO mice could develop severe insulin resistance. To confirm the effects of adipocyte *Becn1* deletion on glucose and insulin sensitivity, we performed a GTT and an ITT. Compared with WT mice, AKO mice showed glucose (Fig. 3*D*) and insulin intolerance (Fig. 3*E*). When we examined insulin signaling pathways, insulin-dependent AKT phosphorylation was found to be significantly reduced in eWAT, liver, and muscles of AKO mice (Fig. 3*F*). Together, these results propose that adipocyte *Becn1* ablation leads to lipodystrophy accompanied by defects in lipid and glucose metabolism as well as insulin sensitivity.

No Defects in Adipocyte Differentiation in *Becn1* AKO Mice

To determine the cause of WAT reduction in AKO, we next investigated whether *Becn1* ablation might affect adipocyte differentiation. As it has been reported that *Becn1* knockdown inhibits lipid droplet formation in 3T3-L1 cells (24), we hypothesized that decreased adiposity in AKO mice might result from defects in adipocyte differentiation. As shown in Fig. 4*A*, *Becn1* AKO showed ~70% reduction of *Becn1* mRNA only in adipocytes, but not in SVCs (Fig. 4*A*). Six days after induction of adipogenic stimuli, when *Becn1* expression was significantly diminished, there was no significant difference in the adipogenic potential of SVC-derived adipocytes from WT and AKO mice, at least in the aspect of lipid accumulation (Fig. 4*B*). Consistently, the mRNA levels of adipogenic genes were not altered by deletion of *Becn1* in adipocytes (Fig. 4*C*). To assess whether *Becn1* can directly modulate the activity of PPARγ, a key transcription factor for adipogenesis, we also conducted luciferase assays in HEK293 cells. As shown in Fig. 4*D* and *E*, there were no changes in PPARγ reporter activity by transient overexpression of BECN1 in the absence or presence of rosiglitazone, the synthetic ligand of PPARγ. Together, these data propose that reduced WAT in AKO mice did not result from impaired adipocyte differentiation.

Cell-Autonomous Death of Adipocytes in *Becn1* AKO Mice

As CLSs were frequently observed in the WAT of AKO mice (Fig. 2*A* and *B*), we asked whether decreased adiposity in AKO mice might be due to enhanced adipocyte death. Since adipose tissue is comprised of various cell types, we assessed adipocyte death by staining the adipocyte-specific lipid droplet binding protein PLIN1/perilipin 1 (25). Compared with WT mice, PLIN1-negative dead adipocytes were abundant in AKO mice (Fig. 5*A*). Similarly, the levels of PLIN1 protein and mRNA were remarkably lower in eWAT

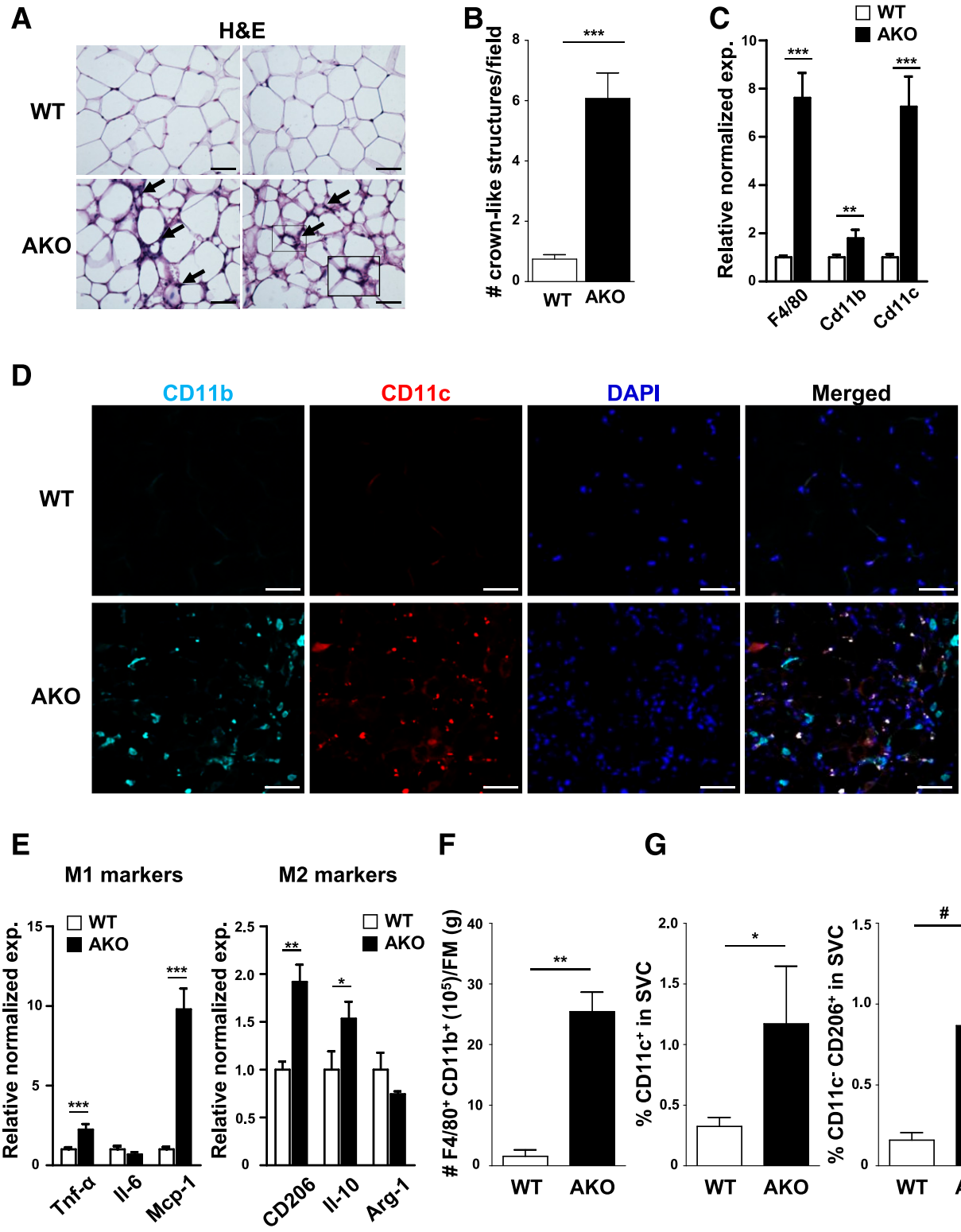

Figure 2—Adipocyte *Becn1* deficiency promotes adipose tissue inflammation. *A*: Histological analysis of eWAT from 10-week-old WT and AKO mice. WAT sections were examined by H&E staining. Black arrows indicate CLSs. Scale bars, 50 μm. *B*: Quantification of CLSs in WT and AKO mice ($n = 8$). *C*: The mRNA expression levels of *F4/80*, *Cd11b*, and *Cd11c* in eWAT from 10-week-old WT and AKO mice ($n = 7$). *D*: Representative immunofluorescence images of eWAT from 10-week-old WT and AKO mice. The eWAT sections were stained with CD11b (cyan) and CD11c (red) antibodies. Nucleus was stained with DAPI (blue). Scale bars, 75 μm. *E*: The mRNA expression of M1 and M2 macrophage–specific markers in eWAT from 10-week-old WT and AKO mice ($n = 7$). *F*: Total number of $F4/80^+CD11b^+$ SVCs per gram of eWAT was determined by flow cytometry in WT and AKO mice ($n = 3$). *G*: The percentages of $CD11c^+$ and $CD11c^-CD206^+$ in $F4/80^+CD11b^+$ cells were measured by flow cytometry in the SVCs of WT and AKO mice ($n = 3$). The qRT-PCR results were normalized to *Ppia*. Data are presented as mean ± SEM. $^*P < 0.05$; $^{**}P < 0.01$; $^{***}P < 0.001$; $\#P = 0.12$. exp., expression; FM, fat mass.

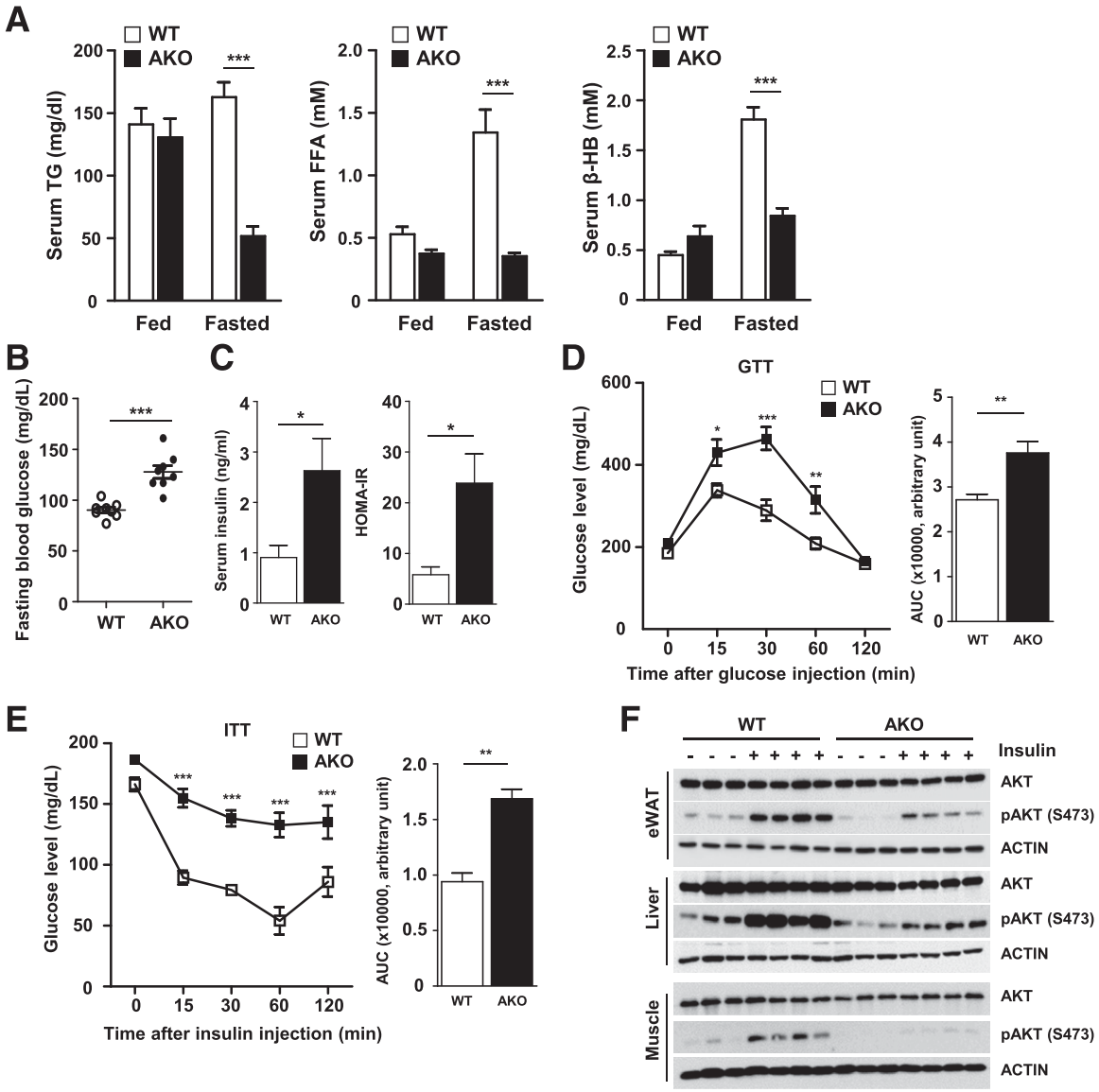

Figure 3—Adipocyte *Becn1* deficiency alters lipid metabolism and decreases insulin sensitivity. *A*: Serum lipid profiles of 12–14-week-old WT and AKO mice in fed ($n = 7$) and fasted ($n = 9$) state. *B*: Fasting blood glucose levels in 10-week-old WT and AKO mice ($n = 8$). *E* (left panel): Serum insulin levels in 10-week-old WT and AKO mice ($n = 8$). *C* (right panel): HOMA of insulin resistance (HOMA-IR) in WT and AKO mice ($n = 8$). *D*: GTT and the area under the curve (AUC) from 10-week-old WT and AKO mice ($n = 6$). *E*: ITT and the AUC from 12-week-old WT and AKO mice ($n = 6$). *F*: Western blot analysis of protein lysates from eWAT, liver, and muscles from 10-week-old WT and AKO mice in response to insulin injection (inj.). Data are presented as mean ± SEM. $^*P < 0.05$; $^{**}P < 0.01$; $^{***}P < 0.001$.

of AKO mice (Fig. 5*B*). In accordance with enhanced adipocyte death in AKO mice, there was a significant increase in the mRNA levels of proapoptotic genes, including *Bax* (~1.8-fold), *Noxa* (~1.9-fold), *Bim* (~1.8-fold), and *Apaf1* (~1.7-fold) in AKO mice (Fig. 5*C*). In eWAT of AKO mice, the levels of BIM, an essential initiator of apoptosis, were upregulated, while BCL2, an antiapoptotic protein, was downregulated (Fig. 5*D*). Increased apoptotic cell death in AKO mice was further confirmed using TUNEL analysis that detects apoptotic DNA fragmentation and 6A7 antibody that recognizes the activated form of BAX, respectively (Fig. 5*E*). These data propose that *Becn1* deficiency in adipose tissue leads to apoptotic cell death via enhanced intrinsic apoptosis pathway. To exclude the possibility that adipocyte death may be caused by a nonautonomous manner (e.g., secretory factors from ATMs), we isolated SVCs from iWAT of WT and AKO mice and treated them to differentiate into adipocytes with adipogenic stimuli. Although there was no difference in the adipogenic potential of SVCs from both genotypes (Fig. 4), we observed ruptured adipocytes with debris in *Becn1*-deficient adipocytes after day 6 (Supplementary Fig. 3), which seemed to be features of adipocyte death (26). In line with this, the number of primary adipocytes stained

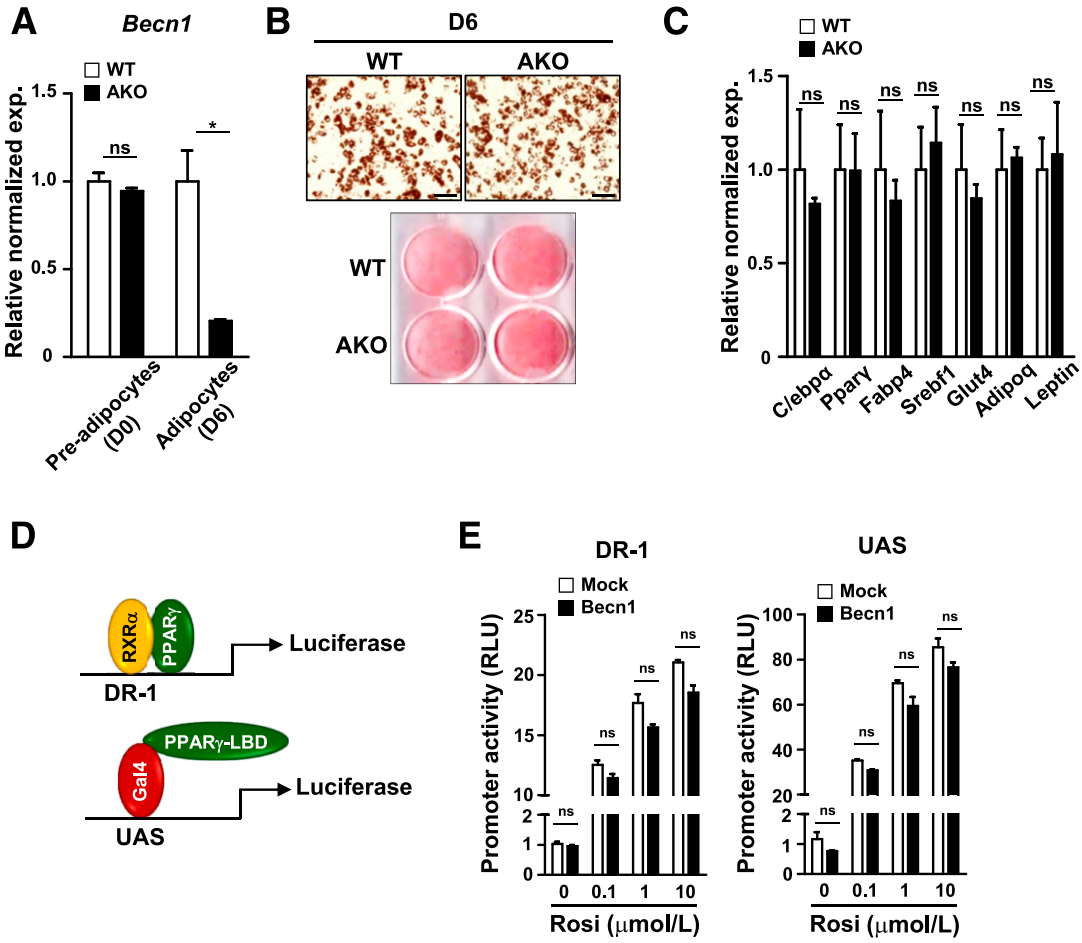

Figure 4—Adipocyte *Becn1* deficiency does not affect adipocyte differentiation in the adipose SVCs. *A*: The mRNA expression (exp.) of *Becn1* in SVCs derived from iWAT of WT and AKO mice without (Preadipocytes) or with (Adipocytes) adipogenic differentiation. The qRT-PCR results were normalized to *Tbp1*. *B*: Oil Red O staining of adipose SVCs derived from iWAT of WT and AKO mice after inducing adipogenic differentiation for 6 days (D6). Scale bars, 100 μm. *C*: The mRNA expression levels of fat differentiation markers in the adipose SVCs derived from iWAT of WT and AKO mice at 6 days after differentiation. The qRT-PCR results were normalized to *Tbp1*. No differences in fat differentiation markers were observed between genotypes. *D*: A schematic representation showing the luciferase reporter constructs. *E*: Effect of *BECN1* on PPARγ activity in HEK293 cells. HEK293 cells were transiently cotransfected with luciferase reporter constructs with human *BECN1* in the absence and presence of rosiglitazone (Rosi). Data are presented as mean ± SEM. *$P < 0.05$. DR1, direct repeat 1; LBD, ligand-binding domain; RLU, relative light unit; UAS, upstream activator sequence.

with propidium iodide was higher in *Becn1*-deficient adipocytes (Fig. 5*F*). Consistent with in vivo results, PLIN1 staining and *Plin1* mRNA levels were significantly decreased in *Becn1*-deficient adipocytes, while the mRNA levels of proapoptotic markers *Bim*, *Bax*, and *Apaf1* were increased (Fig. 5*G* and *H*). Collectively, these results suggest that *Becn1* deficiency in adipose tissue could cause apoptotic adipocyte death in a cell-autonomous manner.

Activation of ER Stress in *Becn1* AKO Mice

To understand the features of adipocyte cell death in AKO mice, we performed microarray analysis in eWAT of WT and AKO mice. Consistent with data above, differentially expressed genes were primarily enriched in gene ontology terms involved in the regulation of apoptotic cell death, cell cycle, autophagy, apoptosis, and immune responses (Fig. 6*A*). Among them, a heat map analysis revealed that ER stress might be related to apoptotic cell death in AKO mice (Fig. 6*B*). Accumulating evidence suggests that activation of autophagy relieves ER stress and prolongs cell survival by reducing misfolded proteins (27,28). Moreover, autophagy defects in pancreatic β-cells lead to extensive ER stress, loss of β-cell mass, and insulin resistance, suggesting an adaptive role of autophagy in the unfolded protein response (UPR) (29,30). Similarly, the mRNA levels of ER stress markers *Grp78/Bip*, *Atf3*, and *Chop* were increased in eWAT of AKO mice (Fig. 6*C*). Western blot analysis also confirmed an increase in the protein levels of p62, GRP78, and CHOP (Fig. 6*D*). Since ER stress markers can be upregulated by indirect pathways of UPR, a dilated ER lumen in eWAT of AKO mice was observed by electron microscopy (Fig. 6*E*), indicating that AKO mice would suffer

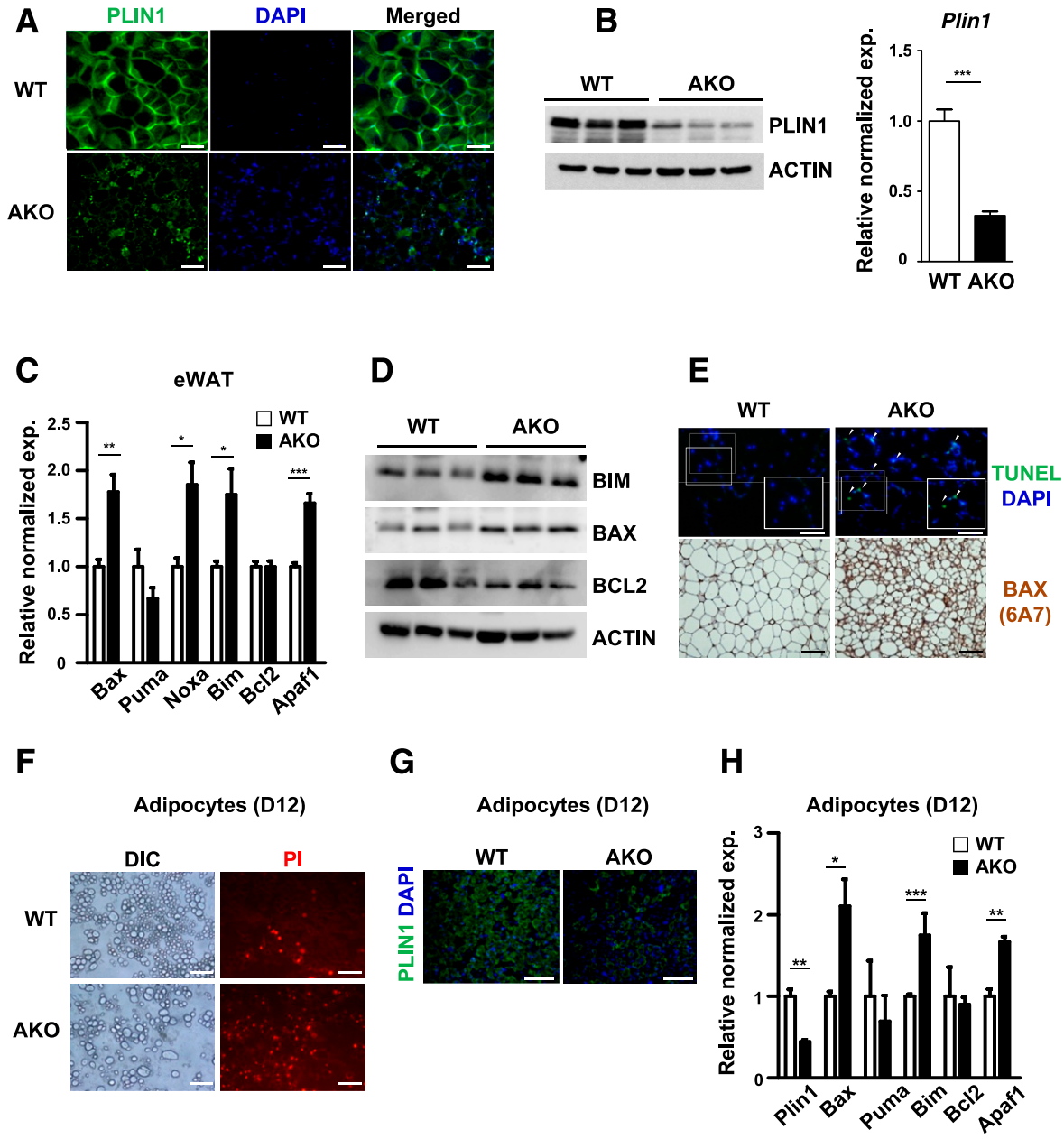

Figure 5—Adipocyte *Becn1* deficiency promotes adipocyte apoptosis in a cell-autonomous manner. *A*: Representative immunofluorescence images of eWAT from 10-week-old WT and AKO mice. The eWAT sections were stained with an antibody to PLIN1 (green). Nucleus was stained with DAPI (blue). Scale bars, 75 μm. *B* (left panel): Western blot analysis of PLIN1 expression in protein lysates from eWAT of WT and KO mice. *B* (right panel): The mRNA expression (exp.) levels of *Plin1* in eWAT from WT and AKO mice ($n = 7$). *C*: The mRNA expression levels of apoptosis markers in eWAT from 10-week-old WT and AKO mice ($n = 7$). *D*: Western blot analysis of BIM, BAX, and BCL2 expression in protein lysates from eWAT of 12-week-old WT and AKO mice. *E*: Detection of adipocyte apoptosis using TUNEL and BAX staining. The eWAT sections were stained with TUNEL and antibody to BAX. White arrowheads indicate TUNEL-positive staining in eWAT of AKO mice. Scale bars, 100 μm. *F*: Fluorescence microscopy of propidium iodide (PI)–stained SVCs derived from iWAT of WT and AKO mice after 12 days (D12) of differentiation. Scale bars, 100 μm. *G*: Immunostaining of PLIN1 in the adipose SVCs derived from WT and AKO mice after 12 days of differentiation. Scale bars, 100 μm. *H*: The mRNA expression levels of *Plin1*, *Bax*, *Puma*, *Bim*, *Bcl2*, and *Apaf1* in the adipose SVCs derived from WT and AKO mice after 12 days of differentiation. The qRT-PCR results were normalized to *Ppia*. Data are presented as mean ± SEM. $^*P < 0.05$; $^{**}P < 0.01$; $^{***}P < 0.001$. DIC, differential interference contrast.

from elevated ER stress. As CHOP is a key transcription factor of ER stress, which promotes severe genes involved in apoptosis (31,32), the mRNA levels of CHOP-related target genes, including *DR5*, *Trib3*, *Gadd34*, and *Ero1α*, were upregulated in eWAT of AKO mice (Fig. 6*F*). To test whether UPR-mediated apoptosis might be involved in *Becn1*-depleted adipocytes, we performed an in vitro analysis of SVCs with a *Becn1* conditional KO system using the *ROSA-Cre*^{ERT2}

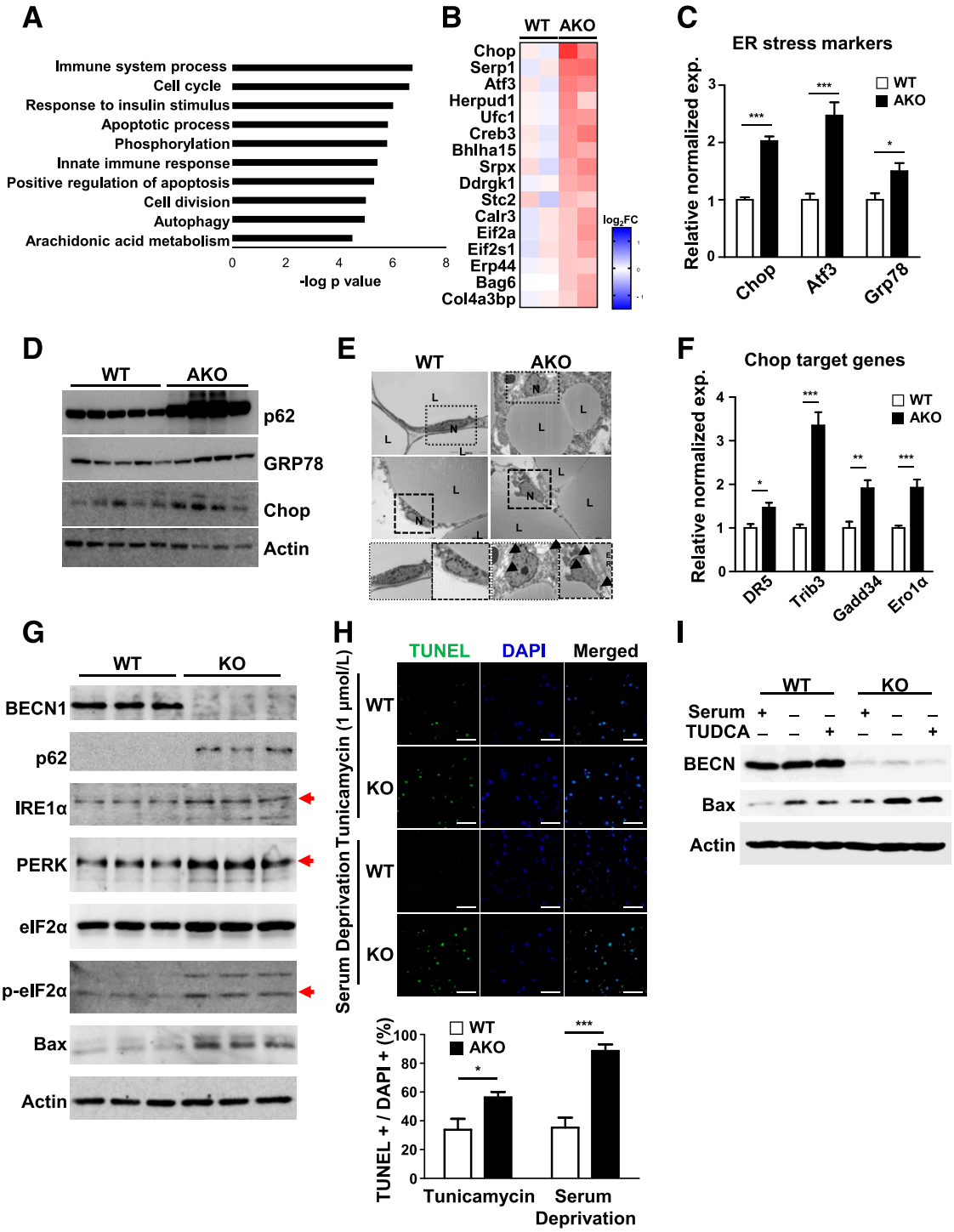

Figure 6—Adipocyte *Becn1* deficiency increases ER stress. *A*: Gene ontology pathways enriched in upregulated genes in eWAT from 10-week-old WT and AKO mice. *B*: Heat map showing expression of genes involved in ER stress response in eWAT from WT and AKO mice. *C*: The mRNA expression (exp.) levels of ER stress markers in eWAT from 10-week-old WT and AKO mice ($n = 7$). *D*: Western blot analysis of p62, GRP78/BIP, and CHOP expression in protein lysates from eWAT of 12-week-old WT and AKO mice. *E*: Transmission electron microscope analysis of eWAT from 10-week-old WT and AKO mice. Black arrows indicate dilated ER. *F*: The mRNA expression levels of *Chop* target genes in eWAT from WT and AKO mice ($n = 7$). *G*: Western blot analysis of ER stress–associated genes in imSVC lines after differentiation. Representative bands of the named proteins are marked with red arrows. *H* (top panel): TUNEL assay of ER stress–induced imSVCs. Tunicamycin (1 μmol/L) or serum-deprived (0%) media was treated to mature adipocytes and incubated 10 days, with media changed every 3 days. *H* (bottom panel): Proportion of TUNEL-positive cells from four distinct confocal microscopy images (original magnification ×40) is shown in bar graphs. Counting TUNEL-positive cells was withheld as a blinded experiment. *I*: Western blot analysis of ER stress–induced and inhibited adipocytes. Serum deprivation–mediated ER stress induction was mitigated by TUDCA (400 μmol/L, 3 days). Band intensity visualized in a bar graph using ImageJ. The qRT-PCR results were normalized to *Ppia*. Data are presented as mean ± SEM. $^*P < 0.05$; $^{**}P < 0.01$; $^{***}P < 0.001$. FC, fold change; L, lipid; N, nucleus.

promoter. SVCs isolated from a mouse mated with *Becn1*$^{f/f}$ and *ROSA-Cre*^{ERT2} were immortalized using simian virus 40 T antigen to establish a cell line (imSVCs). *Becn1* could then be conditionally knocked out upon tamoxifen treatment (Supplementary Fig. 4*A*). To examine the effect of *Becn1* in mature adipocytes, we treated tamoxifen when adipocytes were fully differentiated (day 8). As shown in Fig. 6*G*, we obtained consistent data, as observed in vivo, that imSVCs exhibited enhanced ER stress–induced adipocyte death in the absence of *Becn1*. Among three UPR pathways, imSVCs underwent an elevated PERK-eIF2α-ATF4-CHOP axis as well as IRE1α-mediated Xbp1 mRNA splicing (Fig. 6*G* and Supplementary Fig. 4*B*). Furthermore, to ensure ER stress–mediated adipocyte death would be implicated in Becn1-depleted adipocytes, TUNEL assay was performed in ER stress–induced imSVCs after adipocyte differentiation. When imSVCs were cultured with serum-deprived or tunicamycin-containing media, *Becn1* KO adipocytes were prone to apoptotic death through ER stress accumulation (Fig. 6*H*). In contrast, enhanced adipocyte apoptosis appeared to be downregulated by TUDCA, an inhibitor of ER stress (Fig. 6*I* and Supplementary Fig. 4*C*). Taken together, these data suggest that *Becn1* deficiency in adipose tissue promotes the development of a lipodystrophic phenotype, accompanied by persistent ER stress–mediated adipocyte death.

DISCUSSION

Becn1 plays an important role in cell survival and death as a key regulator of the phosphatidylinositol 3-kinase and BCL-2 complex. Its direct interaction with BCL2 family members such as BIM and BCL2 makes it plausible to be involved in BAX-dependent apoptosis (33). Thus, apart from other autophagy-related proteins such as ATG7, *Becn1*-deficient mice exhibited more severe apoptotic cell death in neurons and embryos, supporting that *Becn1* is associated with cell survival mechanisms distinct from *Atg7*-mediated autophagy (34,35). Nevertheless, as underlying mechanisms by which *Becn1* could affect cell fate are quite complex, this remains controversial. For instance, while *Becn1* contains a proapoptotic BH3 motif that interacts with BCL-2, overexpression of *Becn1* does not induce apoptosis and fails to neutralize antiapoptotic BCL-2 family members (36). However, it has been also reported that *Becn1* has an antiapoptotic role in the TNF-related apoptosis-inducing ligand pathway, chemotherapy, irradiation, immunotherapy, and nutrient deprivation (28). Given that adipocyte cell death is important for adipose tissue homeostasis, how *Becn1* modulates adipocyte survival remains largely unknown.

In this study, we demonstrated that the deletion of adipocyte-specific *Becn1* in AKO mice promoted programmed cell death, adipose tissue inflammation, and insulin resistance, which are common in patients with lipodystrophy (4). AKO mice also exhibited enhanced ER stress, which is observed in obesity-induced apoptosis of adipocytes (37). These features align with the previous study showing that increased adipocyte death is observed with accelerated adipose tissue inflammation, accompanied by insulin resistance (38). Although it has not yet been reported that patients with lipodystrophy have *BECN1* mutations, publicly available genome-wide association study data suggest that variants of *BECN1* are strongly associated with type 2 diabetes and insulin sensitivity (https://www.type2diabetesgenetics.org). However, a direct link between *Becn1* deficiency and adipocyte cell death remains to be investigated.

Given that genetic deletion of core autophagic genes such as *Atg5*, *Atg7*, and *Becn1* results in impaired adipogenesis in mouse embryonic fibroblasts or 3T3-L1 cells (9,24,39), it is widely believed that autophagy is required for adipocyte differentiation by removing unwanted and redundant cellular contents (40). In this study, however, expression levels of the adipogenic markers were uninterrupted by *Becn1* ablation (Fig. 4*C*), implying that reduced adipose tissue mass in AKO mice did not result from altered adipogenic potentials. Of course, our model is not sufficient to investigate how *Becn1* regulates adipocyte differentiation since *Becn1* gene expression in AKO mice would be diminished only when adiponectin expresses via adipoq-Cre. There are some discrepancies between the data obtained from 3T3-L1 cells with knockdown of *Atg* genes and floxed *Atg* mice driven by the Adipoq-*Cre* line. These inconsistencies may not be baffling, if we consider that adiponectin expression increases after adipocyte differentiation. As adipogenesis is a process that consists of a series of steps including lineage commitment, mitotic clonal expansion, growth arrest, and terminal differentiation (41), it is quite complex to discriminate at exactly which steps *Becn1* directly or indirectly affects adipocyte differentiation.

Adipose tissue devoid of *Becn1* showed increased expression of CHOP target genes (Fig. 6*C*). It is known that the accumulation of unfolded proteins in ER activates CHOP and mediates apoptosis (42). Recently, it has been suggested that *Becn1*-mediated hyperactivation of autophagy in insulin-responsive cells increases insulin sensitivity by suppressing ER stress (16), which led us to speculate how *Becn1* deficiency–derived ER stress could initiate apoptosis in adipocytes. Indeed, we observed that *Becn1*-depleted adipocytes exhibited enhanced ER stress–mediated apoptosis (Fig. 6*G* and *H*), implying that persistent induction of ER stress could precede adipocyte death in AKO mice.

It has been reported that deletion of *Atg3* or *Atg16L1* in adipocytes leads to dysfunctional mitochondria, resulting in systemically elevated lipid peroxides (12). While these mice exhibited similar fat mass compared with WT mice, *Becn1* AKO mice exhibited significant reduction of WAT mass regardless of NCD- or HFD-fed conditions (Fig. 1*C* and *D* and Supplementary Fig. 2*B*). Depleting *Becn1* from fully differentiated adipocytes also revealed that they undergo both persistent ER stress and its accumulation. In this study, we can assume that *Becn1* deletion contributes

in a greater magnitude to induce apoptotic response in mature adipocytes. In addition, depletion of *Atg3* led to increased number of CLSs with enhanced F4/80 staining. *Becn1* AKO mice also exhibited similar phenotypes as shown in Fig. 2*A–D*, and further investigation of macrophage polarization found that the ratio of M1/M2 was increased in *Becn1* AKO mice (Fig. 2*E–G* and Supplementary Fig. 3*K* and *L*). These results provide an insight that inflammatory response in adipose tissue could be a common physiological outcome of inhibition of autophagy flux. However, how *Becn1* plays more a influential role in regulating death signals in response to stress compared with other autophagy-related genes remains to be further elucidated.

As the concurrence of ER stress and autophagy is common in several human pathologies, their response is tightly regulated (43). Further delineation of the relationship between ER stress and autophagy revealed a selective elimination of damaged mitochondria through enhanced expression of PARK2, p62, and NBR1, shedding light on the possibility that selective autophagy could emerge through ER stress induction (44,45). *Becn1* being the essential protein for autophagosome formation and autolysosome fusion, *Becn1*-deficient models may experience incompletion of selective autophagy induced by ER stress—especially, as shown from fluorescent reporter mito-Keima, when mitophagy was suppressed in *Becn1*–deficient adipocytes (Supplementary Fig. 5*A* and *B*), which is consistent with the data from Gelmetti et al. (46) that *Becn1* is required for mitophagy completion. Additionally, we observed attenuated mitochondrial potential (Supplementary Fig. 5*C* and *D*) and morphologically abnormal mitochondria in AKO adipocytes (Supplementary Fig. 5*E*). It is likely that suppressed mitophagy by *Becn1* deficiency caused aberrant mitochondria quality control in AKO adipocytes. However, there was little difference in mitochondrial number between two genotypes (Supplementary Fig. 5*F*). Thus, it remains to be elucidated whether inability to alleviate stress due to inhibition of selective autophagy leads to adipocyte death in our mouse model (47–49).

In summary, we show that the deletion of *Becn1* in adipocytes leads to an increase in apoptosis accompanied by ER stress. In addition, AKO mice develop severe lipodystrophy with hepatic steatosis and show a dramatic decline in survival rates with fasting-induced hypothermia, indicating that adipocyte *Becn1* is a crucial regulator of adipose tissue homeostasis.

Funding. This work was supported by National Research Foundation of Korea grants funded by the Korean government (Ministry of Science and ICT, NRF-2020R1A3B2078617 to J.B.K. and 2018R1A2A1A05022746, 2020R1A4A1019063, and 2019R1I1A 01058338) and in part by the Brain Korea 21 PLUS Project for Medical Science.

Duality of Interest. No potential conflicts of interest relevant to this article were reported.

Author Contributions. Y. Jin wrote the manuscript and performed the majority of the experiments. Y. Ji wrote the manuscript and performed the majority of the experiments. Y.S. wrote the manuscript and performed designed experiments. S.S.C. helped designing the experiments. Y.G.J. helped with luciferase assay and microarray data analysis. H. Na helped with mouse management. T.W.N. helped with mouse management. H.J.K. helped with Western blot experiments. H.Nah. conducted FACS analysis. S.M.K. helped with adipocyte differentiation and mouse management. J.-w.K. oversaw the project. K.T.N. helped with immunohistochemistry experiments. J.K.S. helped with indirect calorimetric data analysis. D.H. helped with microarray data analysis. C.B.P. oversaw the project. I.H.L. oversaw the project. J.B.K. and H.-W.L. are the guarantors of this work and, as such, had full access to all of the data in the study and take responsibility for the integrity of the data and the accuracy of the data analysis.

References

1. Ghaben AL, Scherer PE. Adipogenesis and metabolic health. Nat Rev Mol Cell Biol 2019;20:242–258
2. Sun K, Kusminski CM, Scherer PE. Adipose tissue remodeling and obesity. J Clin Invest 2011;121:2094–2101
3. Jung UJ, Choi MS. Obesity and its metabolic complications: the role of adipokines and the relationship between obesity, inflammation, insulin resistance, dyslipidemia and nonalcoholic fatty liver disease. Int J Mol Sci 2014;15:6184–6223
4. Fiorenza CG, Chou SH, Mantzoros CS. Lipodystrophy: pathophysiology and advances in treatment. Nat Rev Endocrinol 2011;7:137–150
5. Baril JG, Junod P, Leblanc R, et al. HIV-associated lipodystrophy syndrome: a review of clinical aspects. Can J Infect Dis Med Microbiol 2005;16:233–243
6. Eren E, Özkan TB, Çakır ED, Sağlam H, Tarım Ö. Acquired generalized lipodystrophy associated with autoimmune hepatitis and low serum C4 level. J Clin Res Pediatr Endocrinol 2010;2:39–42
7. Choe SS, Huh JY, Hwang IJ, Kim JI, Kim JB. Adipose tissue remodeling: its role in energy metabolism and metabolic disorders. Front Endocrinol (Lausanne) 2016;7:30
8. Shimizu S, Kanaseki T, Mizushima N, et al. Role of Bcl-2 family proteins in a non-apoptotic programmed cell death dependent on autophagy genes. Nat Cell Biol 2004;6:1221–1228
9. Singh R, Xiang Y, Wang Y, et al. Autophagy regulates adipose mass and differentiation in mice. J Clin Invest 2009;119:3329–3339
10. Zhang Y, Goldman S, Baerga R, Zhao Y, Komatsu M, Jin S. Adipose-specific deletion of autophagy-related gene 7 (atg7) in mice reveals a role in adipogenesis. Proc Natl Acad Sci U S A 2009;106:19860–19865
11. Altshuler-Keylin S, Shinoda K, Hasegawa Y, et al. Beige adipocyte maintenance is regulated by autophagy-induced mitochondrial clearance. Cell Metab 2016;24:402–419
12. Cai J, Pires KM, Ferhat M, et al. Autophagy ablation in adipocytes induces insulin resistance and reveals roles for lipid peroxide and Nrf2 signaling in adipose-liver crosstalk. Cell Rep 2018;25:1708–1717.e5
13. Wirawan E, Lippens S, Vanden Berghe T, et al. Beclin1: a role in membrane dynamics and beyond. Autophagy 2012;8:6–17
14. Kondo Y, Kanzawa T, Sawaya R, Kondo S. The role of autophagy in cancer development and response to therapy. Nat Rev Cancer 2005;5:726–734
15. He C, Wei Y, Sun K, et al. Beclin 2 functions in autophagy, degradation of G protein-coupled receptors, and metabolism. Cell 2013;154:1085–1099
16. Yamamoto S, Kuramoto K, Wang N, et al. Autophagy differentially regulates insulin production and insulin sensitivity. Cell Rep 2018;23:3286–3299
17. Jin Y, You L, Kim HJ, Lee HW. Telomerase reverse transcriptase contains a BH3-like motif and interacts with BCL-2 family members. Mol Cells 2018;41:684–694
18. Galarraga M, Campión J, Muñoz-Barrutia A, et al. Adiposoft: automated software for the analysis of white adipose tissue cellularity in histological sections. J Lipid Res 2012;53:2791–2796

19. Ham M, Choe SS, Shin KC, et al. Glucose-6-phosphate dehydrogenase deficiency improves insulin resistance with reduced adipose tissue inflammation in obesity. Diabetes 2016;65:2624–2638
20. Huh JY, Park J, Kim JI, Park YJ, Lee YK, Kim JB. Deletion of CD1d in adipocytes aggravates adipose tissue inflammation and insulin resistance in obesity. Diabetes 2017;66:835–847
21. Forman BM, Tontonoz P, Chen J, Brun RP, Spiegelman BM, Evans RM. 15-Deoxy-delta 12, 14-prostaglandin J2 is a ligand for the adipocyte determination factor PPAR gamma. Cell 1995;83:803–812
22. Lumeng CN, Bodzin JL, Saltiel AR. Obesity induces a phenotypic switch in adipose tissue macrophage polarization. J Clin Invest 2007;117:175–184
23. Handelsman Y, Oral EA, Bloomgarden ZT, et al.; American Association of Clinical Endocrinologists. The clinical approach to the detection of lipodystrophy - an AACE consensus statement. Endocr Pract 2013;19:107–116
24. Ro SH, Jung CH, Hahn WS, et al. Distinct functions of Ulk1 and Ulk2 in the regulation of lipid metabolism in adipocytes. Autophagy 2013;9:2103–2114
25. Feng D, Tang Y, Kwon H, et al. High-fat diet-induced adipocyte cell death occurs through a cyclophilin D intrinsic signaling pathway independent of adipose tissue inflammation. Diabetes 2011;60:2134–2143
26. Yeh YS, Jheng HF, Iwase M, et al. The mevalonate pathway is indispensable for adipocyte survival. iScience 2018;9:175–191
27. Ogata M, Hino S, Saito A, et al. Autophagy is activated for cell survival after endoplasmic reticulum stress. Mol Cell Biol 2006;26:9220–9231
28. Bartolome A, Guillen C, Benito M. Autophagy plays a protective role in endoplasmic reticulum stress-mediated pancreatic β cell death. Autophagy 2012; 8:1757–1768
29. Antonucci L, Fagman JB, Kim JY, et al. Basal autophagy maintains pancreatic acinar cell homeostasis and protein synthesis and prevents ER stress. Proc Natl Acad Sci U S A 2015;112:E6166–E6174
30. Jung HS, Chung KW, Won Kim J, et al. Loss of autophagy diminishes pancreatic beta cell mass and function with resultant hyperglycemia. Cell Metab 2008;8:318–324
31. Puthalakath H, O'Reilly LA, Gunn P, et al. ER stress triggers apoptosis by activating BH3-only protein Bim. Cell 2007;129:1337–1349
32. Lee MR, Bae SJ, Kim JE, et al. Inhibition of endoplasmic reticulum stress in high-fat-diet-induced obese C57BL/6 mice: efficacy of a novel extract from mulberry (*Morus alba*) leaves fermented with *Cordyceps militaris*. Lab Anim Res 2018;34:288–294
33. Luo S, Garcia-Arencibia M, Zhao R, et al. Bim inhibits autophagy by recruiting Beclin 1 to microtubules. Mol Cell 2012;47:359–370
34. McKnight NC, Zhong Y, Wold MS, et al. Beclin 1 is required for neuron viability and regulates endosome pathways via the UVRAG-VPS34 complex. PLoS Genet 2014;10:e1004626
35. Kuma A, Komatsu M, Mizushima N. Autophagy-monitoring and autophagy-deficient mice. Autophagy 2017;13:1619–1628
36. Boya P, Kroemer G. Beclin 1: a BH3-only protein that fails to induce apoptosis. Oncogene 2009;28:2125–2127
37. Kawasaki N, Asada R, Saito A, Kanemoto S, Imaizumi K. Obesity-induced endoplasmic reticulum stress causes chronic inflammation in adipose tissue. Sci Rep 2012;2:799
38. Kuroda M, Sakaue H. Adipocyte death and chronic inflammation in obesity. J Med Invest 2017;64:193–196
39. Baerga R, Zhang Y, Chen P-H, Goldman S, Jin S. Targeted deletion of autophagy-related 5 (atg5) impairs adipogenesis in a cellular model and in mice. Autophagy 2009;5:1118–1130
40. Mizushima N, Levine B. Autophagy in mammalian development and differentiation. Nat Cell Biol 2010;12:823–830
41. Chen L, Cui J, Hou J, Long J, Li C, Liu L. A novel negative regulator of adipogenesis: microRNA-363. Stem Cells 2014;32:510–520
42. Nishitoh H. CHOP is a multifunctional transcription factor in the ER stress response. J Biochem 2012;151:217–219
43. Rashid HO, Yadav RK, Kim HR, Chae HJ. ER stress: autophagy induction, inhibition and selection. Autophagy 2015;11:1956–1977
44. Zhang X, Yuan Y, Jiang L, et al. Endoplasmic reticulum stress induced by tunicamycin and thapsigargin protects against transient ischemic brain injury: involvement of PARK2-dependent mitophagy. Autophagy 2014;10:1801–1813
45. Rubio N, Verrax J, Dewaele M, et al. p38(MAPK)-regulated induction of p62 and NBR1 after photodynamic therapy promotes autophagic clearance of ubiquitin aggregates and reduces reactive oxygen species levels by supporting Nrf2-antioxidant signaling. Free Radic Biol Med 2014;67:292–303
46. Gelmetti V, De Rosa P, Torosantucci L, et al. PINK1 and BECN1 relocalize at mitochondria-associated membranes during mitophagy and promote ER-mitochondria tethering and autophagosome formation. Autophagy 2017;13:654–669
47. Kubli DA, Gustafsson AB. Mitochondria and mitophagy: the yin and yang of cell death control. Circ Res 2012;111:1208–1221
48. Schuck S, Gallagher CM, Walter P. ER-phagy mediates selective degradation of endoplasmic reticulum independently of the core autophagy machinery. J Cell Sci 2014;127:4078–4088
49. Lamark T, Johansen T. Aggrephagy: selective disposal of protein aggregates by macroautophagy. Int J Cell Biol 2012;2012:736905